Robust Transcriptional Regulatory Response Upon Blocking NHEJ

Ronald Benjamin (ronald.babu@unlv.edu)
University of Nevada, Las Vegas
Atoshi Banerjee
University of Nevada, Las Vegas
Corey Guerunk
University of Nevada, Las Vegas
Lindsay Buczek
University of Nevada, Las Vegas
Danielle Eames
University of Nevada, Las Vegas
Sara Trimidal
University of Nevada, Las Vegas
Martin Schiller
University of Nevada, Las Vegas

Research Article

Keywords: DNA repair, TALEN, NHEJ, XRCC4(-/-), Mirin

Posted Date: April 30th, 2021

DOI: https://doi.org/10.21203/rs.3.rs-459760/v1

Robust transcriptional regulatory response upon blocking NHEJ

Ronald Benjamin[1*], Atoshi Banerjee[1], Corey Guerunk[1], Lindsay Buczek[1], Danielle Eames[1], Sara Trimidal[1], and Martin R. Schiller[1*]

[1]Nevada Institute of Personalized Medicine and School of Life Science[2], University of Nevada Las Vegas, Las Vegas, Nevada, 89154-4004 United States of America

Corresponding authors: Martin R. Schiller and Ronald Benjamin

Keywords

DNA repair, TALEN, NHEJ, *XRCC4*(-/-), Mirin.

Abstract:

Double strand breaks are one of the most lethal forms of DNA lesions that, if left unrepaired can lead to genomic instability, cellular transformation, and cell death. However, cells have two main machineries namely error prone Non homologous end joining repair (NHEJ) or an accurate homology dependent repair to repair the double strand breaks. NHEJ is the preferred mechanism for DNA repair and basically consists of two forms: Canonical (C-NHEJ) and Alternative (A-NHEJ) NHEJ. Our study examined the cellular repair outcome when NHEJ is blocked by targeting two key DNA repair proteins: XRCC4 and MRE-11. We developed an extrachromosomal NHEJ fluorescent reporter assay that uses Transcription activator-like effector nucleases (TALEN) to introduce double strand breaks and detect the NHEJ editing by the presence of GFP fluorescence. We demonstrated the presence of NHEJ editing in the *XRCC4*(-/-) cells treated with Mirin (a pharmacological inhibitor of MRE-11), albeit with a ~52% efficiency of the normal cells. The transcriptional profiles of the Mirin treated HeLa *XRCC4*(-/-) cells had 307 uniquely differentially expressed genes that was far greater than HeLa *XRCC4*(-/-) sample (83 genes) and Mirin treated HeLa cells (30 genes). Pathway analysis unique to the *XRCC4*(-/-) +Mirin group included differential expression of p53 downstream pathways, and metabolic pathways indicating cell adaptation for energy regulation and stress response. In conclusion, our study showed that the double strand DNA repair can be sustained even in absence of key DNA repair proteins XRCC4 and MRE-11.

Introduction:

DNA carries genetic instructions for the development and function of all known living organisms; therefore, it is important to preserve the integrity of the DNA. However, DNA is not inert, but susceptible to multiple types of damages. The common sources of DNA damage include environmental agents such as UV light, ionizing radiation, and chemical mutagens. Additionally, endogenous biological processes such as cellular metabolism including oxidative damage, DNA alkylation or hydrolysis, and double-strand breaks (DSBs) from collapsed replication forks contributes to DNA damage [1]. In fact every day, DNA in normal cells has approximately 10,000 DNA aberrations and thus require an efficient repair of DNA damage to maintain its integrity [2,3]. Failure to repair such damages can lead to genomic instability, cellular transformation, and cell death.

To mitigate DNA damage and maintain integrity, cells have multiple molecular mechanisms to repair different types of damages. The most deleterious DNA damage is arguably a DSB which, if left unrepaired, threatens the loss of chromosomal content. The key machinery to repair DSBs are (i) Non homologous end joining (NHEJ) repair and (ii) homology dependent repair (HDR) [4]. NHEJ being the predominant form of repair, can commence in any phase of the cell cycle, unlike HDR, which is active during the late S or G2 phase and is a less prevalent form of repair.

A mammalian cell can execute NHEJ repair within approximately 30 min [5], although the disadvantage is that it often introduces indels [6]. The most common form of NHEJ repair is Canonical-NHEJ; catalyzed by two core protein-DNA complexes, Ku70/Ku80/DNA-PKC and DNALig4/XRCC4/XLF-1 [7]. A backup repair pathway called Alternative-NHEJ (A-NHEJ) was identified from persistent NHEJ activity in cells deficient for C-NHEJ [8]. A-NHEJ is evolutionarily

conserved and can act in both C-NHEJ proficient or deficient cells [9]. A-NHEJ can mediate repair with short homology at the site of DNA breaks and is also referred as microhomology dependent DNA repair (MMEJ), although microhomology is not essential [7].

Our earlier *in silico* analysis showed that the gene editing enzymes likely interfere with binding of key components of DNA repair complexes and may alter the preference for C-NHEJ or A-NHEJ [10]. Although XRCC4 and MRE-11 are well studied NHEJ complex proteins, we investigated changes in cellular responses when both C-NHEJ and A-NHEJ are blocked by targeting these proteins. Targeted inhibition of XRCC4, a component of the NHEJ ligation complex should block NHEJ-mediated DNA repair. Schulte-Uentrop et al. demonstrated that knockout of XRCC4, a component of the LIG4/XLF-1/XRCC4 complex renders cells sensitive to DNA damage caused by either ionizing radiation or enzymatic cleavage of genomic DNA [11]. On the other hand, there is a significant evidence supporting the role of MRN complex consisting of three proteins: meiotic recombination 11 protein (MRE-11), RAD50, and Nijmegen breakage syndrome 1 (NBS1; also known as nibrin), in both C-NHEJ and A-NHEJ double strand break repair. The MRN complex is also widely recognized for the role in HDR [12–15]. Depletion of MRE-11 is associated with the reduction in the microhomology based repair in normal cells and inhibits resection in HeLa *XRCC4*(-/-) cells supporting some role in both C-NHEJ and A-NHEJ [16].

Using an NHEJ reporter construct, we show that NHEJ is prevalent even when both XRCC4 and MRE-11 are blocked separately or simultaneously. Furthermore, the transcriptional profiles of the HeLa *XRCC4*(-/-) cells treated with Mirin, a pharmacological inhibitor of MRE-11 had 307 uniquely differential expressed genes, much higher than the HeLa-NT (control), *XRCC4(-/-)* HeLa and Mirin treated HeLa cells. The inhibition of XRCC4 and MRE-11 was associated with

differential expression of p53 downstream pathways, and metabolic pathways indicating adaptation of the cells to target regulation of energy and stress upon NHEJ inhibition. Our experiments are the first to investigate broad cellular response when NHEJ is inhibited.

Materials and methods

NHEJ reporter plasmid construction

For construction of an NHEJ reporter plasmid, the sequence corresponding to a TALEN binding site (Fig. 1A) was PCR amplified from pLai.2 HIV proviral plasmid (NIH AIDS Reagent Program #2532) and cloned upstream of the mCherry coding sequence into the NheI and AgeI sites of the pmCherry-C1 plasmid (Takara #632524). For cloning a TALEN binding site (TBS) downstream of the mCherry coding sequence, the TBS was amplified, fused with GFP coding sequence by overlap-PCR and cloned between the SalI and BamHI restriction enzyme sites. The coding sequence of EGFP was amplified from the plasmid pEGFP-C3. A spacer was introduced between the cytomegalovirus promoter (CMV) promoter and the upstream TBS at the NheI restriction enzyme site (New England Biolabs) within the pmCherry-C1. Primers used for sequencing and cloning are listed in (Supplementary Table 1).

Cell culture and Lentivirus production

HeLa (ARP 154) cells obtained from the NIH AIDS reagent program and LentiX293T cells (Clonetech# 632180) were grown in Dulbecco modified Eagle's Medium (DMEM) supplemented with 10% FetalClone III Serum (HyClone# SH30109.03). Lentivirus was produced from transfected LentiX293T cells. Briefly, 6 well plates were seeded with 0.6 million cells and incubated for 24 hrs prior to transfection. Cells were co-transfected with gXRCC4-lenticrisprV2/gScrambled-lenticrisprV2, 1.2 µg; pspax-2 (Addgene. # 12260), 1.0 µg, and pVSVG

(Addgene. # 22501), 0.3 μg using the Lipofectamine LTX transfection reagent (Invitrogen) at a 1:3 ratio [DNA(μg): Transfection reagent(μl)]. After 6 hrs of incubation, media was replaced, and cells were cultured in complete media for 48 hours. Cell supernatant were collected, filtered through a 0.45 μm syringe filter (Millipore), and used for transduction into HeLa cells.

Assessment of NHEJ repair

TALEN expression constructs (TAL 256 and TAL 278) were previously constructed with the Joung Lab REAL Assembly TALEN kit [17,18]. To assess DNA repair, HeLa cells (0.6 million) were seeded a day before transfection, co-transfected with a NHEJ reporter plasmid and pairs of TALEN expressing constructs [TAL 256 (200 ng) and TAL 278 (200 ng)] at a ratio of 1:3 [DNA(μg): Transfection reagent(μl)] with Viafect transfection reagent (Promega). As a control, NHEJ reporter plasmid was co-transfected with empty vector [JDS70 (200ng) and JDS 78 (200ng)]. Media was changed after 4 hrs incubation and replaced with complete media with or without Mirin (Sigma, 100 μM). After 48 hours, cells were tested for mCherry and GFP fluorescence by fluorescence microscopy and flow cytometry.

Generation of a *XRCC4* knockout cell line – HeLa *XRCC4*(-/-)

To generate a *XRCC4*(-/-) HeLa cell line, a gXRCC4 sequence targeting the *XRCC4* gene (NCBI RefSeq: NC_000005.10) was annealed, phosphorylated with T4 Polynucleotide Kinase (New England Biolabs) and cloned into the BsmBI digested LenticrisprV2 plasmid (Addgene # 52961)). The plasmid was delivered into HeLa cells by lentiviral transduction. The cells were selected in complete media with puromycin (1.5 μg/ml) for 1 week followed by clonal selection. Clonal cells were screened for biallelic *XRCC4* knockout by Western Blotting with a XRCC4 antibody (Santa Cruz Biotechnology sc-271087) on Nitrocellulose membrane (GE Amersham) and by targeted

sequencing of gDNA. One of the clones 2G3 (HeLa *XRCC4*(-/-)) was selected for all subsequent experiments. For the control HeLa cells, non-targeting guide RNA was similarly expressed in HeLa cells. Genomic DNA (gDNA) was isolated from HeLa *XRCC4(*-/-) and HeLa-NT (control cell containing non-targeting gRNA) using Quick DNA plus Kit (Zymogen). Isolated gDNA spanning the selected region of the *XRCC4* gene (NCBI RefSeq: NC_000005.10 (83104920.-83105621)) was amplified by PCR with XRCC4-SeqV2FP and RA-XRCC4seq-RP primers and Herculase II Fusion DNA polymerase (Agilent). PCR amplified product was digested with XhoI (New England Biolabs), and subcloned into the XhoI and EcoRV restriction enzyme sites of the pBlueScript II SK (-) vector. Several colonies were screened for the XRCC4 gDNA insert, and *XRCC4* knockout for the 2G3 clonal cells were confirmed by sanger sequencing.

MTT assay for metabolic activity

Cells were analysed with a 3-(4,5-dimethylthiazol-2-yl)-2,5-diphenyltetrazolium bromide (MTT) chromogenic metabolic activity assay. HeLa-NT and *XRCC4*(-/-) cells were cultured in 96-well plates for one day and an additional two days with complete media (DMEM+ 10% FetalClone SerumIII) with or without Mirin dissolved in Dimethyl sulfoxide (DMSO, 100 μM). DMSO vehicle control was added to the control cells. Media was removed and 50 μl of incomplete media (DMEM) with 50 μl MTT (5 mg/ml) was added to each well and incubated for 4 h at 37°C in a CO_2 incubator. Resulting formazan crystals were dissolved with 100 μl of acidified isopropanol, incubated for 5 min at 37 °C, and absorbance at 595 nm was measured with a DTX 880 multimode detector (Beckman Coulter).

Fluorescence Microscopy

Transfected cells were cultured for 48 hours before measuring fluorescence. Live cells were scored for EGFP and mCherry fluorescence in fresh media. Images were acquired at 20X magnification with a Nikon TE2000E epifluorescence microscope equipped with Photometrics CoolSNAP FX Camera (Roper Scientific). Images were captured in sequential scanning mode to avoid spectral bleed through and were analysed in triplicates with multiple scanning regions for each.

Fluorescent Activated Cell Sorting (FACS)

Transfected cells were cultured for 48 hours before FACS analysis. Cells were trypsinized, washed twice with phosphate buffered saline (PBS) and fixed with 2% paraformaldehyde for 10 min at RT. Cells were washed twice with PBS before acquisition with a flow cytometer (Sony SH800). Cells were gated first for mCherry expression followed by GFP expression. Experiments were analysed using FlowJo 10.7.1 for triplicate samples.

RNA-seq and data processing

Cells were transfected with a NHEJ reported plasmid and TALEN constructs and treated with Mirin or vehicle control after 4 hrs post transfection. Cells were harvested 48 hrs after transfection and total RNA was extracted with the Zymogen RNA prep kit (Zymogen). Duplicate samples for each condition were analyzed. RNA was quantified, RNA-seq was performed at a depth of more than 20 million paired end reads for each sample (Novagene Corporation Inc).

The RNA-seq data can be accessed at Gene Expression Omnibus (GEO) (accession no GSE135274). For RNA-seq analysis, raw reads were imported into CLC Genomics Workbench 12.0 and trimmed using the quality limit score of 0.05 calculated from a modified-Mott trimming algorithm [19], read through adapter trimming, and trimming of ambiguous bases from read regions

with more than two ambiguous reads [19]. RNA-Seq analysis was performed using default settings including a mismatch cost of 2 with insertion and deletion cost of 3. The Reference genome was hg19 and reference gene track used was ensemble_v74. Differential expression analysis was performed with the Identify and Annotate Differentially Expressed Genes (DEGs) software.

Bioinformatic analysis

A principal component analysis (PCA) of RNA-seq data and resulting plot were created with ClustVis (https://biit.cs.ut.ee/clustvis/) [20]. Venn Diagrams of differentially expressed genes for each condition was compared to control (FDR<0.01 log FC>=1) and plotted with an online tool (http://bioinformatics.psb.ugent.be/webtools/Venn/). Heatmaps for the DEGs were plotted using the Heatmap.2 function in the R ggplot package R (Warnes et al., 2020). Volcano plots for each category were created using "EnhancedVolcano" function in R [21]. Gene enrichment analysis was performed for DEGs lists (FDR<0.01 and logFC>1.2) with Metascape [22]. A network graph was created with Cytoscape (v3.1.2). Term relationships having a similarity score above 0.3 are connected by edges. The network is visualized with Cytoscape (v3.1.2).

Protein–protein interaction (PPI) network analysis and pathways interrelation analysis

PPI networks were constructed using multiple DEGs list based on BioGrid, InWeb_IN and OmniPath database in Metascape. For networks which contain between 3-500 proteins, Molecular Complex Detection (MCODE) algorithm was used to identify densely connected network components with default parameters. For each MCODE component, pathway and process enrichment analysis was applied and the three best-scoring (by p value) terms were retained as the functional description of the resulting modules. Resulting network graphs were visualized through Cytoscape (v3.1.2).

Quantitative Real-time Polymerase Chain Reaction (qRT-PCR)

For validation of RNA-seq results, cells were transfected with a NHEJ reported plasmid, TALEN expression constructs, and treated with Mirin or vehicle control as described above. Cells were harvested 48 hrs after transfection, Total RNA was extracted using the Zymogen RNA prep kit (Zymogen) and cDNA was synthesized with SuperScript™ IV VILO™ Master Mix (Invitrogen). Gene expression of select DEGs were quantified by qRT-PCR with gene-specific primers (Table S1), and PowerUp SYBR Green PCRmix (Invitrogen) in a Bio-Rad CFX96 Touch™ Real-Time PCR Detection System. Relative expression levels were normalized to a housekeeping control gene. *β-actin*. The fold changes in mRNA levels between the HeLa-NT and the experimental condition were calculated using the $2^{-(\Delta\Delta CT)}$ method.

Statistical Analyses

Statistical analyses were conducted with Student's *t*-test or by ANNOVA for comparing more than 2 groups and a p-value ≤ 0.05 was considered significant.

Results

Construction and validation of a NHEJ reporter assay

In order to test and detect NHEJ repair when TALEN introduces DSBs, we first constructed and tested a plasmid encoding an extrachromosomal NHEJ reporter assay system. The reporter plasmid has a CMV promoter for constitutive expression of the mCherry coding sequence. The mCherry coding sequence is flanked on either side with TBSs (Fig. 1A). Under normal conditions, the mCherry reading frame terminates with a stop codon. Consequently, the downstream GFP coding sequence lacks a promoter; hence not expressed. When the cells are co-transfected with the

reporter plasmid and the pair of TALEN expressing plasmids, that targets the encoded TBSs, double strand breaks are introduced at both TBSs excising the mCherry coding region. Upon subsequent NHEJ repair, the CMV promotor is ligated in proximity to the GFP coding region driving its expression. Therefore, GFP is expressed upon NHEJ repair. A flow chart depicting the relationships between DNA editing and fluorescence output is shown (Fig. 1A).

First, we tested the NHEJ reporter assay system in HeLa cells. The reporter plasmid was co-transfected with TALEN expression constructs T256 and T278. GFP positive (GFP^+) cells were detected indicating editing by NHEJ (Fig. 1B). Co-transfection of the NHEJ reporter plasmid with empty vectors, or with either one of the TALEN pair did not express any GFP^+ cells as expected for cells that are not edited (Fig. 1B). This experiment confirms that our NHEJ assay system is functional, specific, sensitive, and detects DNA repair.

Inhibition of XRCC4 and MRE-11 in Hela cells

To determine the effect of XRCC4 and MRE-11 on C-NHEJ and A-NHEJ repair pathways, we needed to abolish expression of these proteins. *XRCC4* was knocked out in Hela cells using targeted CRISPR-Cas9 editing within the coding region. The *XRCC4*(-/-) biallelic knockout in clone 2G3 was confirmed by the loss of XRCC4 protein expression as detected by Western blot analysis (Fig. 1C). A complete absence of XRCC4 protein expression was observed, and this clone was selected for further experiments. The knockout in clone 2G3 was confirmed by Sanger sequencing, which revealed a 2 bp deletion and 10 bp deletion at both the alleles in the *XRCC4* gene (Fig. 1D). MRE-11 expression was indispensable for cell survival thus, MRE-11 was inhibited by Mirin, a well-established inhibitor of MRN complex and MRE-11 exonuclease activity. We also analyzed the cell survival when *XRCC4*(-/-) cells were treated with Mirin (Fig.

1E). Blocking both XRCC4 and MRE-11 indicate that that the cells are viable as detected in an MTT assay (Fig. 1E).

NHEJ repair is sustained when XRCC4 and MRE-11 are blocked

Since cells with both *XRCC4*(-/-) and MRE-11 blocked survived and were metabolically active, we next assessed the impact of blocking NHEJ on DNA repair activity. *XRCC4*(-/-) and control cells HeLa-NT (Non-targeting) transfected with reporter plasmid and empty TALEN vectors did not show any GFP^+ cells as expected for these negative controls (Fig. 2A & E). Mirin treatment of these cells also had no effect on GFP expression (Fig. 2B & F). mCherry expression indicated that the cells were expressing the reporter construct (Fig. 2). HeLa-NT and *XRCC4*(-/-) cells co-transfected with the NHEJ reporter and TALEN constructs (T270 and T278) showed GFP expression, indicating NHEJ repair (Fig. 2C & G).

In co-transfected HeLa-NT cells treated with Mirin, GFP^+ cells were present indicating NHEJ repair when MRE11 is inhibited (Fig. 2D). Surprisingly, co-transfected Mirin treated *XRCC4*(-/-) also showed NHEJ repair as indicated by the presence of GFP expression (Fig 2 H). This suggests that NHEJ repair is sustained even when XRCC4 and MRE-11 are inhibited.

NHEJ efficiency was lowered when both XRCC4 and MRE-11 are blocked

To quantify the NHEJ repair efficiency, cells expressing the fluorescent reporters were quantified by flow cytometry. Cells were first gated based on $mCherry^+$ expression, selecting the population expressing the reporter system. Next, we determined percentage of cells expressing GFP within the $mCherry^+$ cell populations (Fig. 3A, B). The mean percentage of GFP^+ expressing cells within the $mCherry^+$ cells for each sample is compared in Fig. 3B. The efficiency of NHEJ repair was

(25.5% ± 1.3) in HeLa-NT cells and (15.4% ± 0.4) for HeLa-NT cells treated with Mirin (Fig. 3B), indicating that blocking MRE11 activity reduced NHEJ editing efficiency. Similar inhibition of NHEJ editing was observed in *XRCC4*(-/-) cells (15.9% ± 0.2) or those treated with Mirin (13.26% ± 0.2). These results indicated that NHEJ repair was prevalent even when either or both XRCC4 and MRE-11 are blocked, however; the efficiency is reduced by approximately 40-48%.

Altered expression of genes when NHEJ is blocked

The reporter assay demonstrates that NHEJ repair is partially inhibited, but still present in cells when XRCC4 and MRE-11 expression is blocked alone, as well as in combination. To assess the molecule basis for the robustness in preservation of NHEJ activity, gene expression of transcriptomes was compared for cells with inhibition of XRCC4 and MRE-11. To determine differences in transcriptomes, cell populations selected as above were analyzed by RNA-seq. A principle component analysis showed a clear separation between each sample category, but clustering for duplicate samples (Fig. 4A), indicating a different transcriptomic profile for each sample category.

The transcriptional changes are summarized in a Venn diagram to codify similar and unique genes among samples. The *XRCC4*(-/-) sample had 83 and Mirin treated HeLa cells had 30 unique differentially expressed genes (Fig. 4B). However, the Mirin treated *XRCC4*(-/-) cells had 307 uniquely differentially expressed genes, far greater than other samples reflecting a more impactful transcriptional response. This differential transcriptional response was further supported when the top differentially expressed genes (DEGs) were plotted as heatmap (Fig.4C and Supplementary Table 2). The gene expression for *XRCC4(*-/-) cells treated with Mirin were most different from HeLa-NT cells (Fig. 4C). To validate the gene expression quantitation, five differentially

expressed genes identified from the RNA-seq analysis (*CA9, CDKN1A, ENO2, DUSP5 and ZMAT3*) were assessed by real time PCR. The top differentially expressed genes plotted for heatmap (Fig. 4) and the p53 downstream pathway were selected for gene expression quantitation by real time PCR (Fig. 5A). The PCR data and RNA-seq gene expression measurements were consistent with each other, thereby validating the RNA-seq results (Supplementary Fig. 1). The cells with either *XRCC4* knock out or treated with Mirin showed fewer and less intense changes in gene expression. Additional details for changes in gene expression are shown by volcano plots in Supplementary Fig 2.

Pathway analysis of differentially expressed genes (DEGs)

We next sought to determine which pathways are functionally associated with the transcriptional response to blocking NHEJ. DEG enrichment was analyzed with Metascape [22]. Meta-enrichment analysis indicated that all 3 conditions with partially or completely blocked NHEJ were consistently enriched in several pathways: transcriptional misregulation in cancer, alcoholism, defense response to viruses, and response to oxygen levels (Fig. 5A). Pathways unique to *XRCC4*(-/-) cells with or without Mirin were Extracellular matrix organization, core matrisome, and endoderm and fat differentiation pathways (Fig. 5A). Pathways like carboxylic acid biosynthetic process, p53 downstream pathways and HIF signaling pathway were enriched in *XRCC4*(-/-) + Mirin group and in HeLa-NT treated with Mirin. Interestingly, pathways unique to *XRCC4*(-/-) with Mirin group were regulation of small metabolic processes, TP53 regulates transcription of cell death gene, generation of precursor metabolites and energy (Fig. 5A). A network layout was created by enrichment analysis and visualized with Cytoscape (v3.1.2) (Fig. 5B). Such network reveals interrelation of enriched pathways and genes.

PPI network construction and pathways interaction analysis

Pathways were also evaluated by examining protein-protein interaction networks. A protein-protein interaction network was constructed from the DEGs for the 3 sample conditions with BioGrid in Metascape [22]. The network contained a total of 237 nodes and 956 edges where network nodes are displayed as pies (Fig. 6A). Seven significant network modules were identified with the MCODE algorithm (Fig. 6B), which included 71 proteins from which ENO3, CACNG6, ITGB8, PDE10A, COL12A1 and FSTL3 served as seed proteins. Gene Ontology (GO) terms associated with each module are depicted in Fig. 6B and HDAC deacetylates histones appear to be the prominent GO term. As expected, human histone acetylation and deacetylation regulate the NHEJ repair pathways [23].

DISCUSSION

There are two NHEJ repair pathways for repairing DSBs upon DNA damage. We sought to better understand the relationship between these pathways. First, we designed, tested, and validated a NHEJ reporter construct that enabled us to examine the cells that have undergone NHEJ mediated DNA repair. When *XRCC4* is knocked out or MRE-11 exonuclease activity is inhibited, NHEJ mediated DNA repair was reduced by ~40%. Interestingly, NHEJ activity was reduced to ~50% in *XRCC4(-/-)* + Mirin treated cells compared to wild type HeLa-NT cells. We predicted that blocking NHEJ would increase vulnerability to cell death due to reduced ability to repair DNA damage. This observation indicates that NHEJ is sustained, even when XRCC4 and MRE-11 and presumably the functions of the know NHEJ pathways are abolished. These observations support NHEJ pathways with redundant functions, that may be mediated by a transcriptional response.

We considered three possible explanations for the presence of NHEJ repair despite inhibiting XRCC4 and MRE-11: 1) There could be a yet to be discovered NHEJ pathway. However, this possibility is unlikely considering that the comparative transcriptomic profiles did not reveal any differential expression of DNA repair proteins or components of DNA repair complexes. We recognize that this negative result is not conclusive, as is the case for any negative result. However, analysis of whole transcriptome is a global measurement, but there could be genes with repair functions that are not yet identified or annotated; 2) Another possible explanation is that either MRE-11 or XRCC4 have other genes that can compensate for the lack of their functions. Although Xing et al., identified *PAXX*, a new paralogue of *XRCC4* [24], this gene was not differentially expressed in our case; and 3). Another possibility, which we favor is that post translational modifications of known DNA repair proteins or new protein-protein interactions modulate NHEJ pathways and the changes in post-translational regulation would not be captured by the RNA-seq analysis.

Considering the latter hypothesis, our DEG analysis identified multiple pathways that were induced for each condition that block NHEJ. The result suggests induction of a substantial regulatory response that may produce signaling cross talk between the NHEJ repair pathways. Although, NHEJ is the major repair pathway for DSB; the temporal recruitment of different factors and complexes are not completely elucidated. It is likely that MRE-11 may function upstream of the XRCC4 involvement in the DNA repair and may suggest interaction between these NHEJ pathways.

In support of cross-talk hypothesis, studies on cross talk of NHEJ with base excision repair (BER) and HDR with some common proteins were identified [25,26]. Xia et al. has demonstrated that Polβ

383 which plays a central role in BER, exhibits higher degree of spatial colocalization with Ku70, a
384 component of C-NHEJ in the nucleus following DNA damage caused by Methyl methanesulfonate
385 or etoposide [27]. *In vitro* binding assays also supports interaction between Polβ and Ku70. MRE-11
386 has a critical role in DSB recognition and protein complex recruitment in both the NHEJ and HR
387 pathways. Another protein, BRCA-1, is known to regulate the nuclease activity of MRE-11.
388 BRCA1 phosphorylation mediated by Checkpoint kinase-2- enhances NHEJ fidelity but can also
389 deplete 53BP in S/G2 phase to favor HR, suggesting that post-translation modification of BRCA1
390 regulates pathway preference [25,26]. Thus, it is possible that both C-NHEJ and A-NHEJ could also
391 have signaling interactions that rescue blocking both NHEJ pathways [9,28].
392
393 One theme that emerged from blocking NHEJ was that blocking of NHEJ pathways by either
394 *XRCC4* knock out or Mirin treatment alone or in combination lead to pathways like transcriptional
395 misregulation in cancer, alcoholism, defense response to viruses, and response to oxygen levels.
396 The error prone nature of NHEJ is a major cause of carcinogenesis and blocking of these pathways
397 in our experiments correlates with the transcriptional misregulation associated with cancer
398 pathway. Introduction of DSB/viral DNA leads to activated DNA repair pathway components
399 which are also activated as a defense response to viruses [29]. Similarly, oxidative stress induces
400 DNA damage and activate NHEJ mediated pathways [30]. Enrichment of these pathways highlight
401 cellular adaptation in response to DNA damage.
402
403 Although, we did not identify any major DNA repair protein to be uniquely altered in double
404 inhibition of XRCC4 and MRE-11 in cells, a bypass pathway may utilize some proteins already
405 known to be associated with NHEJ. The pathways enriched in these cells include pathways
406 associated with regulation of small molecule metabolic processes, TP53 regulates transcription of

cell death genes and generation of precursor metabolites and energy suggesting a major role played by genes of metabolic pathway in such a scenario. The metabolic enzymes are known to play non-canonical roles outside their established metabolic roles especially in gene regulation, DNA damage response and apoptosis [31]. Among the metabolic pathway, genes belonging to glycolysis were more prevalent and were downregulated. Induction of glycolysis contributes to enhancement of NHEJ repair pathway and here we show that *XRCC4(-/-)* with Mirin treated cells had lower expression of glycolytic genes, *PGK1, ALDOC, PFKFB4, TPI1, ENO3, PFKP, ENO2, HK2,* when compared to control HeLa-NT cells [32]. However, whether there is a feedback loop mechanism between glycolysis and DNA repair pathway and its potential role in NHEJ will require further investigation.

Depletion of another DNA repair enzyme, DNA-PKc is previously shown to cause alteration in metabolic pathway and TP53 levels [33]. Enhanced p53 activity is a critical cellular signal for DNA damage. Under normal condition, p53 remains in an inactivated state. However, in response to DNA damage, the p53 is activated and drives transcription of factors involved in the apoptosis, cell cycle, DNA repair, and cellular senescence [34,35]. Therefore, to compensate for defective XRCC4 and MRE11, our results show that the metabolic and p53 pathways are altered as an adaption to cellular stress introduced by DSB and in absence of efficient NHEJ repair systems.

A protein-protein interaction network analysis suggest interconnectivity between the transcriptional responses for each NHEJ group (Fig 6A). This is consistent with our hypothesis of cross talk between different NHEJ pathways. While the previously discussed p53 response has an well-known connection with DNA damage and repair, chromatin modifications may be required to give NHEJ repair proteins access to the DSB. One major DEG category supports a possible role

for chromatin modification as part of the regulator response to blocking NHEJ. A set of histones genes that were identified in the protein-protein interaction studies, and these genes are also part of Alcoholism pathway that is highly enriched in the *XRCC4(-/-)* cells treated with Mirin (Fig. 6B). HDACs deacetylation histones have a major influence on chromatin structure and regulates the activation of DNA repair proteins [36]. Therefore, the DEG for these pathways was not surprising. There are several reports supporting the profiles of histone acetylation affecting NHEJ [37–40]. HDAC inhibitors impair DNA repair, suggesting that upregulation of HDAC deacetylation contributes to DNA repair in Mirin treated *XRCC4*(-/-) cells [41].

In conclusion, our results demonstrate that NHEJ is robust, even when key proteins thought to be essential for the two known NHEJ pathways are blocked. Surprisingly, the majority of NHEJ activity was preserved with a corresponding transcriptional response. These results are an important step forward in identifying regulatory interactions between NHEJ pathways.

Authors contribution

RB and MRS conceived the hypotheses and experiments. ST helped collect and analyze literature editing data. RB, AB conducted the experiments and analyzed the data, LB and DE helped with sequencing of *XRCC4*(-/-) cells, CG and XW collected and processed the RNA-seq raw data, RB, AB and MRS contributed to writing of the manuscript and MRS provided funding and space for the work.

Conflict of interest

The authors declare that there are no conflicts of interest.

Funding

The Nevada Governor's office of Economic Development and by the National Institutes of Health (R56 AI109156 and P20 GM121325 to MRS) funded this research. This research is also supported by the Prabhu Endowed Professorship to MRS.

Acknowledgements

Flow cytometry and initial RNA-seq data analyses were performed with resources from the Nevada Institute of Personalized Medicine (NIPM) and the National Supercomputing Institute at University of Nevada Las Vegas (UNLV). The authors would like to acknowledge Edwin Oh and Shirley Shen and Genome Acquisition and Analysis (GAA) Core from the NIH Center of Biomedical Research Excellence (COBRE) at NIPM. Real time PCR was performed at UNLV genomics core facility and is acknowledged.

References

1. Hakem, R. DNA-damage repair; the good, the bad, and the ugly. *EMBO J* **27**, 589–605 (2008).
2. Lindahl, T. Instability and decay of the primary structure of DNA. *Nature* **362**, 709–715 (1993).
3. Peterson, C. L. & Côté, J. Cellular machineries for chromosomal DNA repair. *Genes Dev.* **18**, 602–616 (2004).
4. Mao, Z., Bozzella, M., Seluanov, A. & Gorbunova, V. Comparison of nonhomologous end joining and homologous recombination in human cells. *DNA Repair (Amst)* **7**, 1765–1771 (2008).

5. Mao, Z., Bozzella, M., Seluanov, A. & Gorbunova, V. Comparison of nonhomologous end joining and homologous recombination in human cells. *DNA Repair (Amst)* **7**, 1765–1771 (2008).
6. Rodgers, K. & McVey, M. Error-prone repair of DNA double-strand breaks. *J Cell Physiol* **231**, 15–24 (2016).
7. Sishc, B. J. & Davis, A. J. The Role of the Core Non-Homologous End Joining Factors in Carcinogenesis and Cancer. *Cancers (Basel)* **9**, (2017).
8. Kabotyanski, E. B., Gomelsky, L., Han, J.-O., Roth, D. B. & Stamato, T. D. Double-strand break repair in Ku86- and XRCC4-deficient cells. *Nucleic Acids Research* **26**, 5333–5342 (1998).
9. Deriano, L. & Roth, D. B. Modernizing the nonhomologous end-joining repertoire: alternative and classical NHEJ share the stage. *Annu Rev Genet* **47**, 433–455 (2013).
10. Trimidal, S. G. *et al.* Can Designer Indels Be Tailored by Gene Editing? *Bioessays* **41**, e1900126 (2019).
11. Schulte-Uentrop, L., El-Awady, R. A., Schliecker, L., Willers, H. & Dahm-Daphi, J. Distinct roles of XRCC4 and Ku80 in non-homologous end-joining of endonuclease- and ionizing radiation-induced DNA double-strand breaks. *Nucleic Acids Res* **36**, 2561–2569 (2008).
12. Uziel, T. *et al.* Requirement of the MRN complex for ATM activation by DNA damage. *EMBO J* **22**, 5612–5621 (2003).
13. Zha, S., Boboila, C. & Alt, F. W. Mre11: roles in DNA repair beyond homologous recombination. *Nat Struct Mol Biol* **16**, 798–800 (2009).
14. Stracker, T. H. & Petrini, J. H. J. The MRE11 complex: starting from the ends. *Nat Rev Mol Cell Biol* **12**, 90–103 (2011).

15. Shibata, A. *et al.* DNA double-strand break repair pathway choice is directed by distinct MRE11 nuclease activities. *Mol Cell* **53**, 7–18 (2014).
16. Xie, A., Kwok, A. & Scully, R. Role of mammalian Mre11 in classical and alternative nonhomologous end joining. *Nat Struct Mol Biol* **16**, 814–818 (2009).
17. Miller, J. C. *et al.* A TALE nuclease architecture for efficient genome editing. *Nat. Biotechnol.* **29**, 143–148 (2011).
18. Strong, C. L. *et al.* Damaging the Integrated HIV Proviral DNA with TALENs. *PLoS ONE* **10**, e0125652 (2015).
19. Ewing, B., Hillier, L., Wendl, M. C. & Green, P. Base-calling of automated sequencer traces using phred. I. Accuracy assessment. *Genome Res.* **8**, 175–185 (1998).
20. Metsalu, T. & Vilo, J. ClustVis: a web tool for visualizing clustering of multivariate data using Principal Component Analysis and heatmap. *Nucleic Acids Research* **43**, W566–W570 (2015).
21. Blighe, K. *kevinblighe/EnhancedVolcano*. (2020).
22. Zhou, Y. *et al.* Metascape provides a biologist-oriented resource for the analysis of systems-level datasets. *Nature Communications* **10**, 1523 (2019).
23. Miller, K. M. *et al.* Human HDAC1 and HDAC2 function in the DNA-damage response to promote DNA nonhomologous end-joining. *Nature Structural & Molecular Biology* **17**, 1144–1151 (2010).
24. Xing, M. *et al.* Interactome analysis identifies a new paralogue of XRCC4 in non-homologous end joining DNA repair pathway. *Nature Communications* **6**, 6233 (2015).
25. Daley, J. M. & Sung, P. 53BP1, BRCA1, and the Choice between Recombination and End Joining at DNA Double-Strand Breaks. *Mol Cell Biol* **34**, 1380–1388 (2014).

524 26. Shrivastav, M., De Haro, L. P. & Nickoloff, J. A. Regulation of DNA double-strand break
525 repair pathway choice. *Cell Research* **18**, 134–147 (2008).
526 27. Xia, W. *et al.* Two-way crosstalk between BER and c-NHEJ repair pathway is mediated by
527 Pol-β and Ku70. *FASEB J* **33**, 11668–11681 (2019).
528 28. Shamanna, R. A. *et al.* WRN regulates pathway choice between classical and alternative
529 non-homologous end joining. *Nat Commun* **7**, (2016).
530 29. Hristova, D. B., Lauer, K. B. & Ferguson, B. J. Viral interactions with non-homologous end-
531 joining: a game of hide-and-seek. *Journal of General Virology,* **101**, 1133–1144 (2020).
532 30. Sharma, V. *et al.* Oxidative stress at low levels can induce clustered DNA lesions leading to
533 NHEJ mediated mutations. *Oncotarget* **7**, 25377–25390 (2016).
534 31. Huangyang, P. & Simon, M. C. Hidden features: exploring the non-canonical functions of
535 metabolic enzymes. *Dis Model Mech* **11**, (2018).
536 32. Bhatt, A. N. *et al.* Transient elevation of glycolysis confers radio-resistance by facilitating
537 DNA repair in cells. *BMC Cancer* **15**, 335 (2015).
538 33. Ali, S. I., Najaf-Panah, M. J., Sena, J., Schilkey, F. D. & Ashley, A. K. Comparative gene
539 expression in cells competent in or lacking DNA-PKcs kinase activity following etoposide
540 exposure reveal differences in gene expression associated with histone modifications,
541 inflammation, cell cycle regulation, Wnt signaling, and differentiation. *bioRxiv*
542 2020.09.17.300129 (2020) doi:10.1101/2020.09.17.300129.
543 34. Nd, L. & Sp, J. Regulation of p53 in response to DNA damage. *Oncogene* vol. 18
544 https://pubmed.ncbi.nlm.nih.gov/10618704/ (1999).
545 35. Mijit, M., Caracciolo, V., Melillo, A., Amicarelli, F. & Giordano, A. Role of p53 in the
546 Regulation of Cellular Senescence. *Biomolecules* **10**, (2020).

36. Piekna-Przybylska, D., Bambara, R. A. & Balakrishnan, L. Acetylation regulates DNA repair mechanisms in human cells. *Cell Cycle* **15**, 1506–1517 (2016).
37. Tamburini, B. A. & Tyler, J. K. Localized histone acetylation and deacetylation triggered by the homologous recombination pathway of double-strand DNA repair. *Mol Cell Biol* **25**, 4903–4913 (2005).
38. Jazayeri, A., McAinsh, A. D. & Jackson, S. P. Saccharomyces cerevisiae Sin3p facilitates DNA double-strand break repair. *Proc Natl Acad Sci U S A* **101**, 1644–1649 (2004).
39. Martin, S. G., Laroche, T., Suka, N., Grunstein, M. & Gasser, S. M. Relocalization of telomeric Ku and SIR proteins in response to DNA strand breaks in yeast. *Cell* **97**, 621–633 (1999).
40. Mills, K. D., Sinclair, D. A. & Guarente, L. MEC1-dependent redistribution of the Sir3 silencing protein from telomeres to DNA double-strand breaks. *Cell* **97**, 609–620 (1999).
41. Munshi, A. *et al.* Histone deacetylase inhibitors radiosensitize human melanoma cells by suppressing DNA repair activity. *Clin Cancer Res* **11**, 4912–4922 (2005).

Figure legends:

Figure 1: Construction and validation of NHEJ reporter system

A) Schematic representation of NHEJ reporter system and plausible outcome when both NHEJ pathways are blocked, where TBS = TALEN binding site; CMV = cytomegalovirus promoter. B) Fluorescent microscopy validation of reporter system. C) Western blot confirmation of *XRCC4 (-/-)* clonal selection in HeLa cells where 2G3 clone had no expression. D) Sequence of region of XRCC4 genomic DNA alleles for wild type cells and *XRCC4*(-/-) 2G3 clone. Deletions are indicated by "-". 2G3 clone alleles have a frameshift indel, thus are a biallelic knockout. F) MTT assay of HeLa-NT cells treated with 100 mM of Mirin when compared to HeLa-NT cells. Statistically significant differences were determined by an ANOVA analysis where *denotes $p<0.05$.

Figure 2: DNA double stand break repair when both XRCC4 and MRE-11 are blocked.

Representative fluorescence microscopy images of NHEJ editing when C-NHEJ and A-NHEJ are blocked. HeLa-NT (A-D) and *XRCC4*(-/-) (E-H). Cells co-transfected with TALEN reporter plasmid (expressing mCherry) along with either empty vector or TALEN plasmids where GFP^+ cells indicate DNA repair events and treated with 100uM Mirin wherever indicated. Cells were analyzed 48 hrs post-transfection and representative images are shown. TALEN reporter with empty vector (A, E), empty vector with Mirin (B, F), TALEN plasmid (C, G), TALEN plasmid with Mirin (D, H) are shown.

Figure 3: Measurement of NHEJ efficiency using flow cytometry.

A) Representative images of cells positive for mCherry expression followed by GFP^+ expression. B) Mean GFP^+ cells were plotted. Experiments were done in triplicates and data was analysed using FLowJo 10.7.1. Statistical significance was determined by ANOVA where * indicates $p < 0.01$

Figure 4: Principal component analysis (PCA), Venn Diagram and Heatmap from RNA-seq profile.

A) A PCA plot for HeLa-NT, *XRCC4(-/-),* Mirin and *XRCC4(-/-)*+ Mirin from whole-transcriptome RNA-seq data using ClusVis [20]. B) A Venn diagram representing shared and unique DEGs across 3 categories (i) *XRCC4(-/-)* (blue) (iii) Mirin treated (green) (iii) *XRCC4*(-/-) with Mirin treated (red) when compared to HeLa-NT cells. C) A heatmap of top DEGs across each sample categories.

Figure 5: Functional enrichment analysis

A) A heatmap with embedded dendogram showing relationships between enriched GO/KEGG terms and canonical pathways. 0.3 kappa score was applied as the threshold to cast the tree into term clusters.

B) A network graph with enrichment ontology clusters colored by cluster ID. Each term is represented by a node, where its size is proportional to the number of genes for each term. Terms with a similarity score > 0.3 are linked by an edge (the thickness of the edge represents the similarity score). The network was created with Cytoscape (v3.1.2).

Figure 6: Protein-protein interaction network analysis.

A) PPI network of DEGs across all three NHEJ categories. Nodes are displayed as pies to indicate NHEJ sample. B) MCODE components were identified from merged network for all samples.

Each MCODE network is assigned a unique color and the network was generated with Cytoscape (v3.1.2). C) MCODE GO term, description and p values are shown.

Supplementary Figure 1: Validation of RNA-seq profile across all the categories.

Changes in gene expression determined by real time PCR. The data were represented as mean ± SD and significance between groups were determined by ANOVA test where denoted $p < 0.05$ and NS=not significant.

Supplementary Figure S2: Volcano chart and functional enrichment analysis.

Volcano chart showing differentially expressed genes with FDR<0.01 and logFC>=1.2 compared to HeLa-NT cells A) *XRCC4*(-/-), B) Mirin treatment, C) *XRCC4(-/-)* with Mirin treatment.

Figures

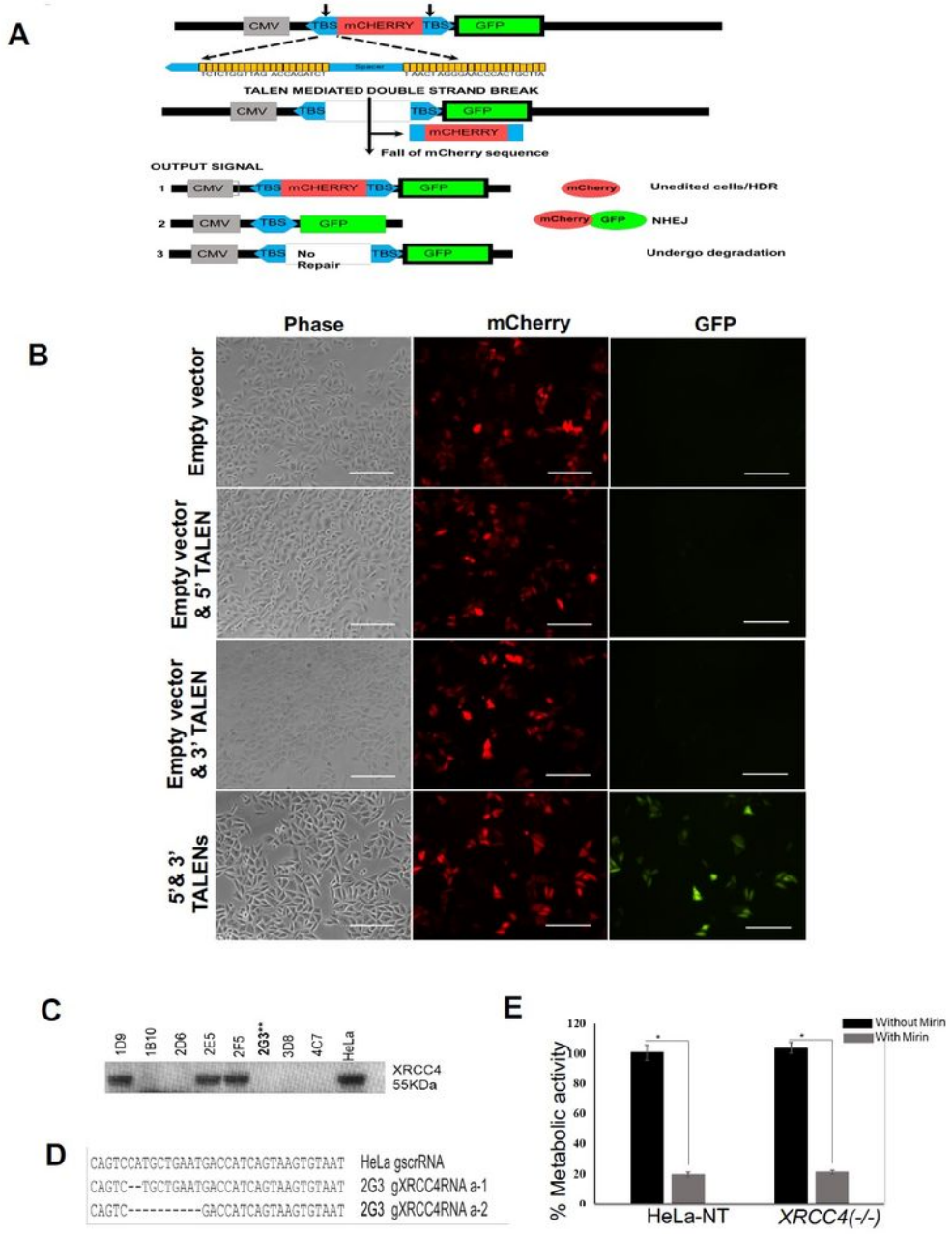

Figure 1

Construction and validation of NHEJ reporter system A) Schematic representation of NHEJ reporter system and plausible outcome when both NHEJ pathways are blocked, where TBS = TALEN binding site; CMV = cytomegalovirus promoter. B) Fluorescent microscopy validation of reporter system. C) Western

blot confirmation of XRCC4 (- /-) clonal selection in HeLa cells where 2G3 clone had no expression. D) Sequence of region of XRCC4 genomic DNA alleles for wild type cells and XRCC4(-/-) 2G3 clone. Deletions are indicated by "-". 2G3 clone alleles have a frameshift indel, thus are a biallelic knockout. F) MTT assay of HeLa-NT cells treated with 100 mM of Mirin when compared to HeLa-NT cells. Statistically significant differences were determined by an ANOVA analysis where *denotes $p<0.05$.

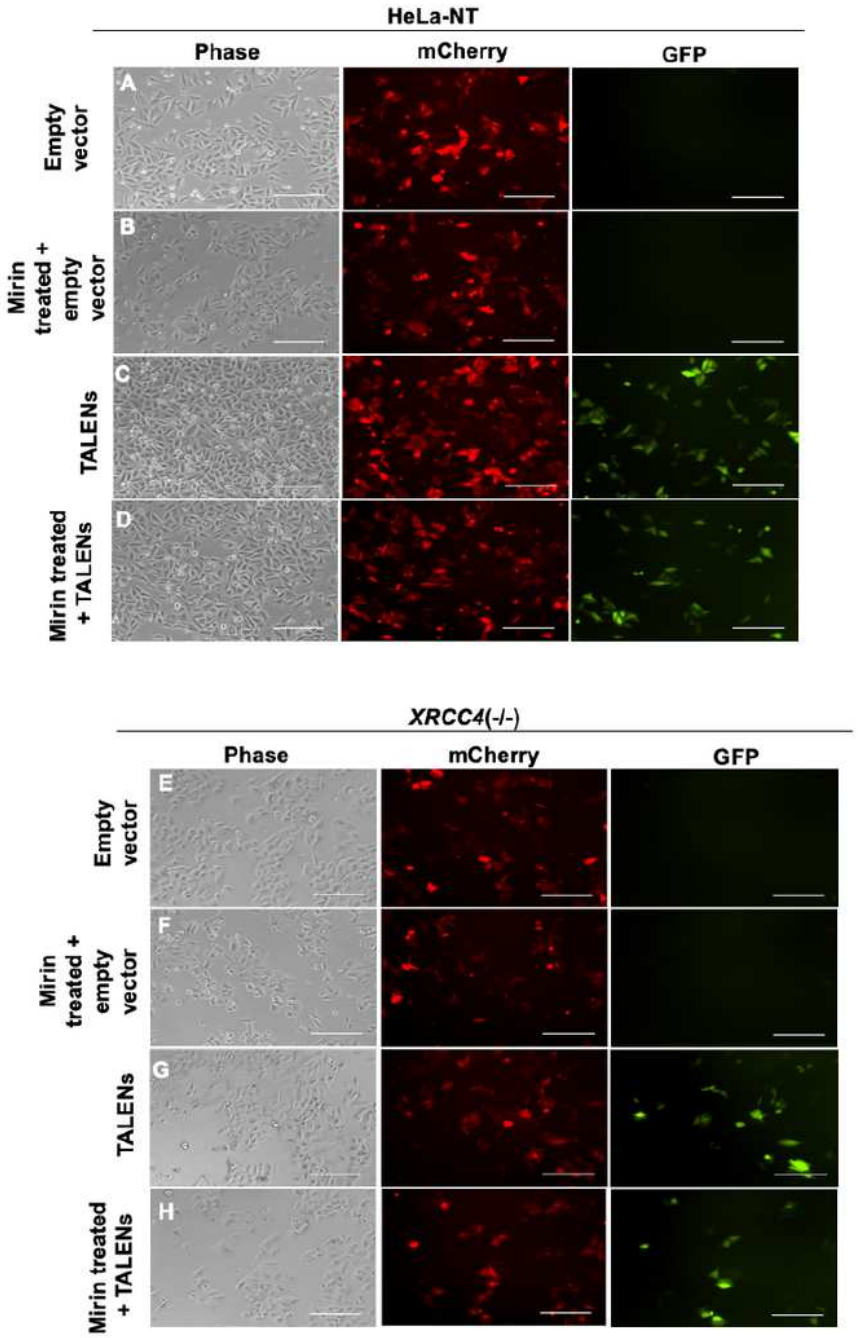

Figure 2

DNA double stand break repair when both XRCC4 and MRE-11 are blocked. Representative fluorescence microscopy images of NHEJ editing when C-NHEJ and A-NHEJ are blocked. HeLa-NT (A-D) and XRCC4(-/-) (E-H). Cells co-transfected with TALEN reporter plasmid (expressing mCherry) along with either empty vector or TALEN plasmids where GFP+ cells indicate DNA repair events and treated with 100uM Mirin wherever indicated. Cells were analyzed 48 hrs post-transfection and representative images are shown. TALEN reporter with empty vector (A, E), empty vector with Mirin (B, F), TALEN plasmid (C, G), TALEN plasmid with Mirin (D, H) are shown.

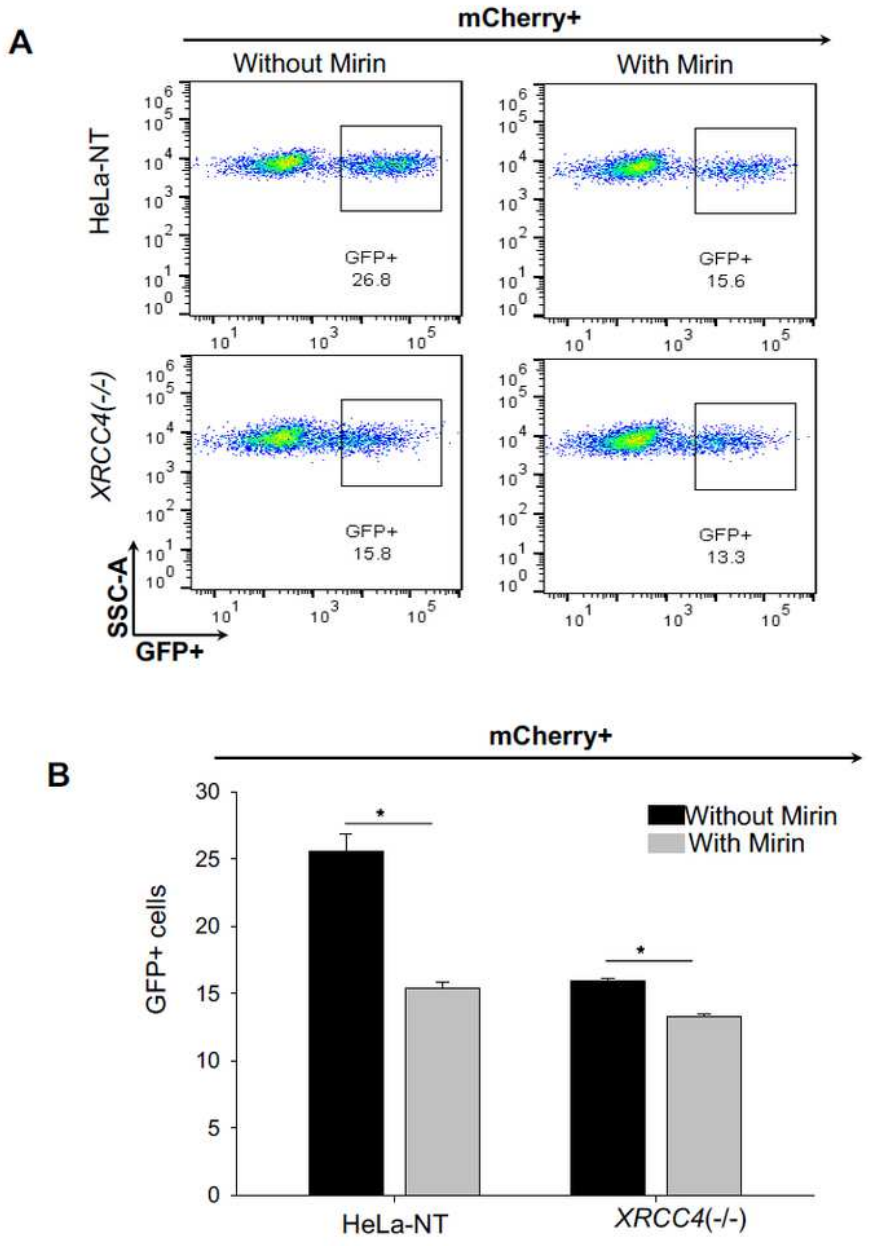

Figure 3

Measurement of NHEJ efficiency using flow cytometry. A) Representative images of cells positive for mCherry expression followed by GFP+ expression. B) Mean GFP+ cells were plotted. Experiments were done in triplicates and data was analysed using FLowJo 10.7.1. Statistical significance was determined by ANOVA where indicates p <0.01

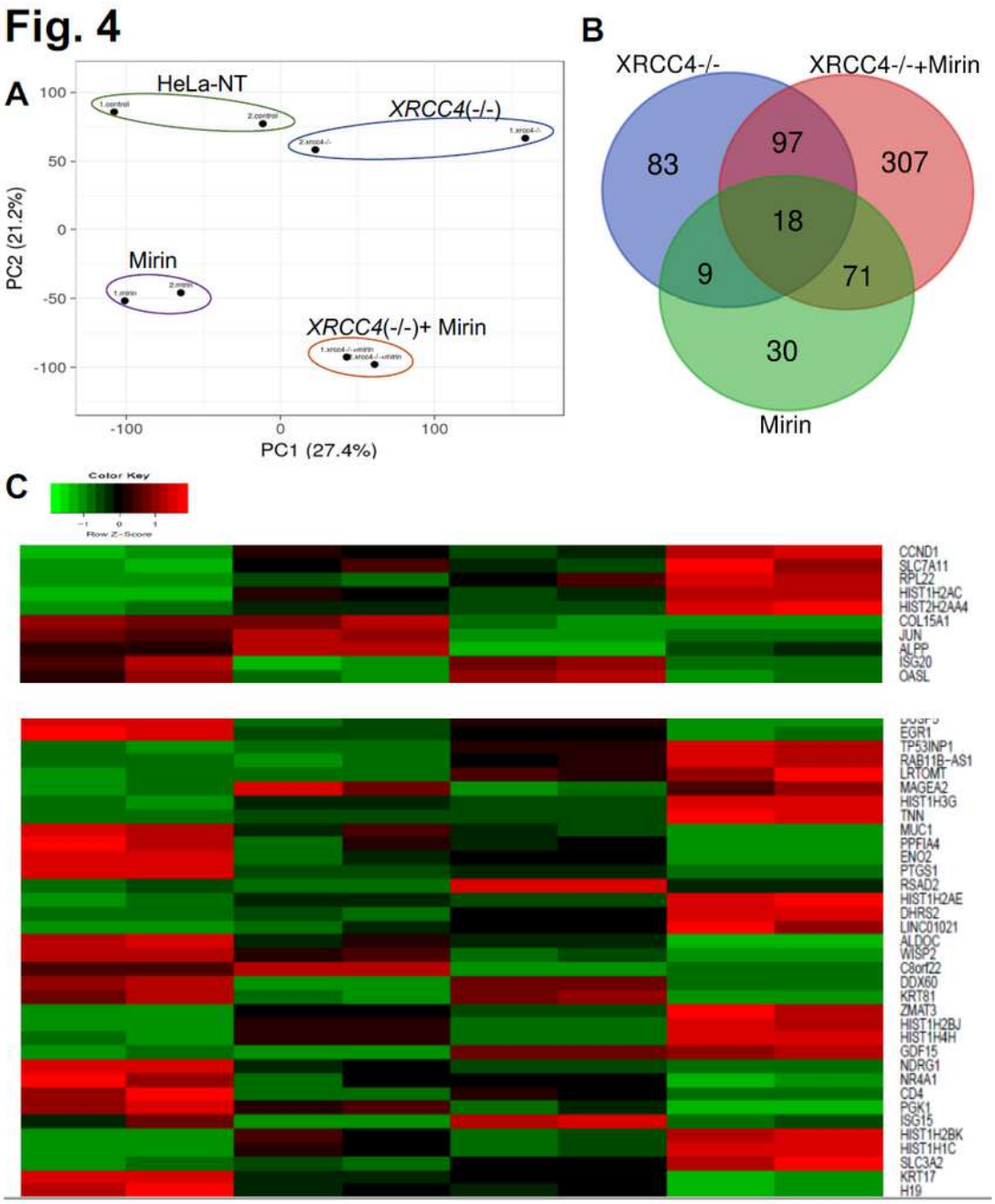

Figure 4

Principal component analysis (PCA), Venn Diagram and Heatmap from RNA-seq profile. A) A PCA plot for HeLa-NT, XRCC4(-/-), Mirin and XRCC4(-/-)+ Mirin from whole transcriptome RNA-seq data using ClusVis 20. B) A Venn diagram representing shared and unique DEGs across 3 categories (i) XRCC4(-/-) (blue) (iii) Mirin treated (green) (iii) XRCC4(-/-) with Mirin treated (red) when compared to HeLa-NT cells. C) A heatmap of top DEGs across each sample categories.

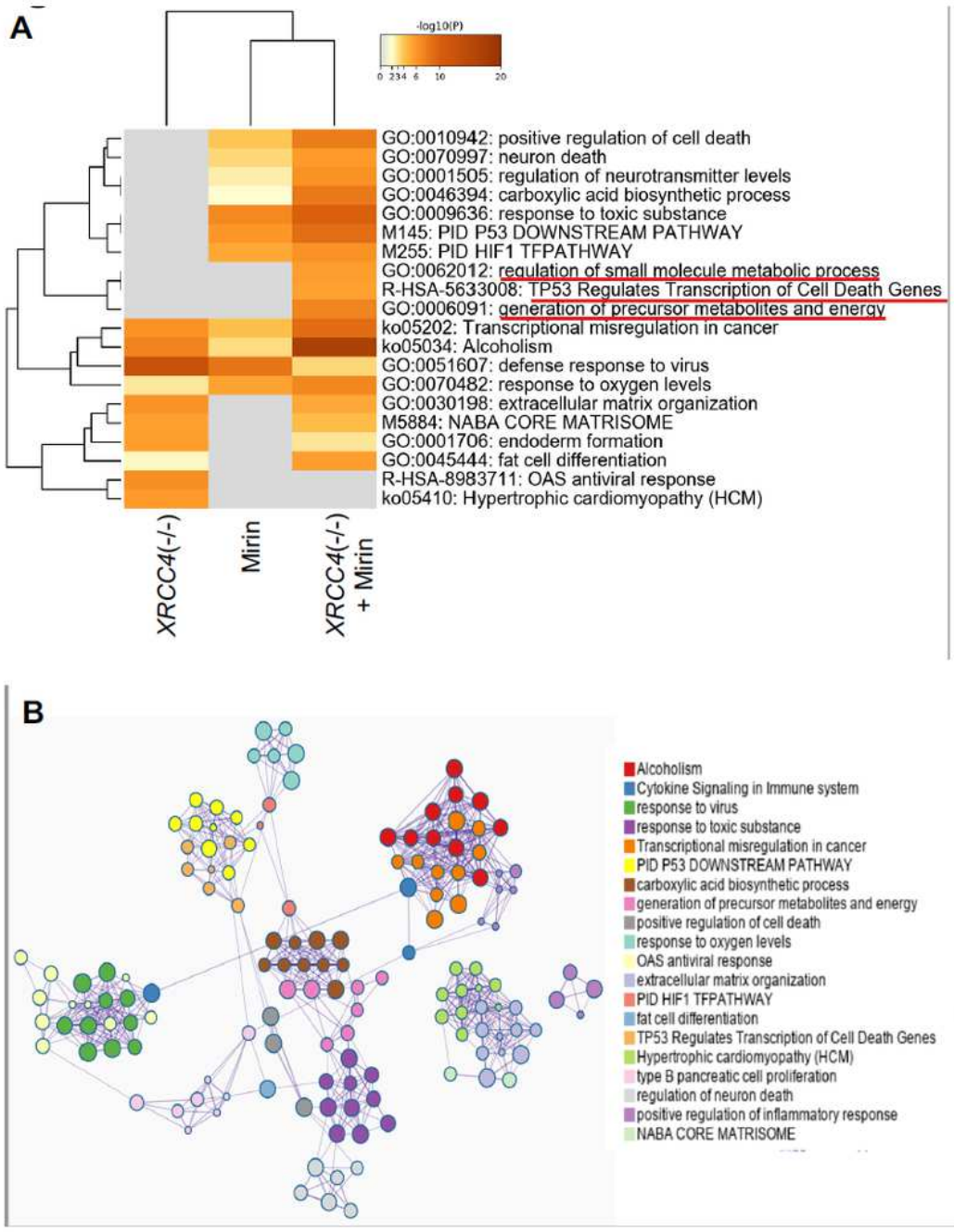

Figure 5

Functional enrichment analysis A) A heatmap with embedded dendogram showing relationships between enriched GO/KEGG terms and canonical pathways. 0.3 kappa score was applied as the threshold to cast the tree into term clusters. B) A network graph with enrichment ontology clusters colored by cluster ID. Each term is represented by a node, where its size is proportional to the number of genes for each term. Terms with a similarity score > 0.3 are linked by an edge (the thickness of the edge represents the similarity score). The network was created with Cytoscape (v3.1.2).

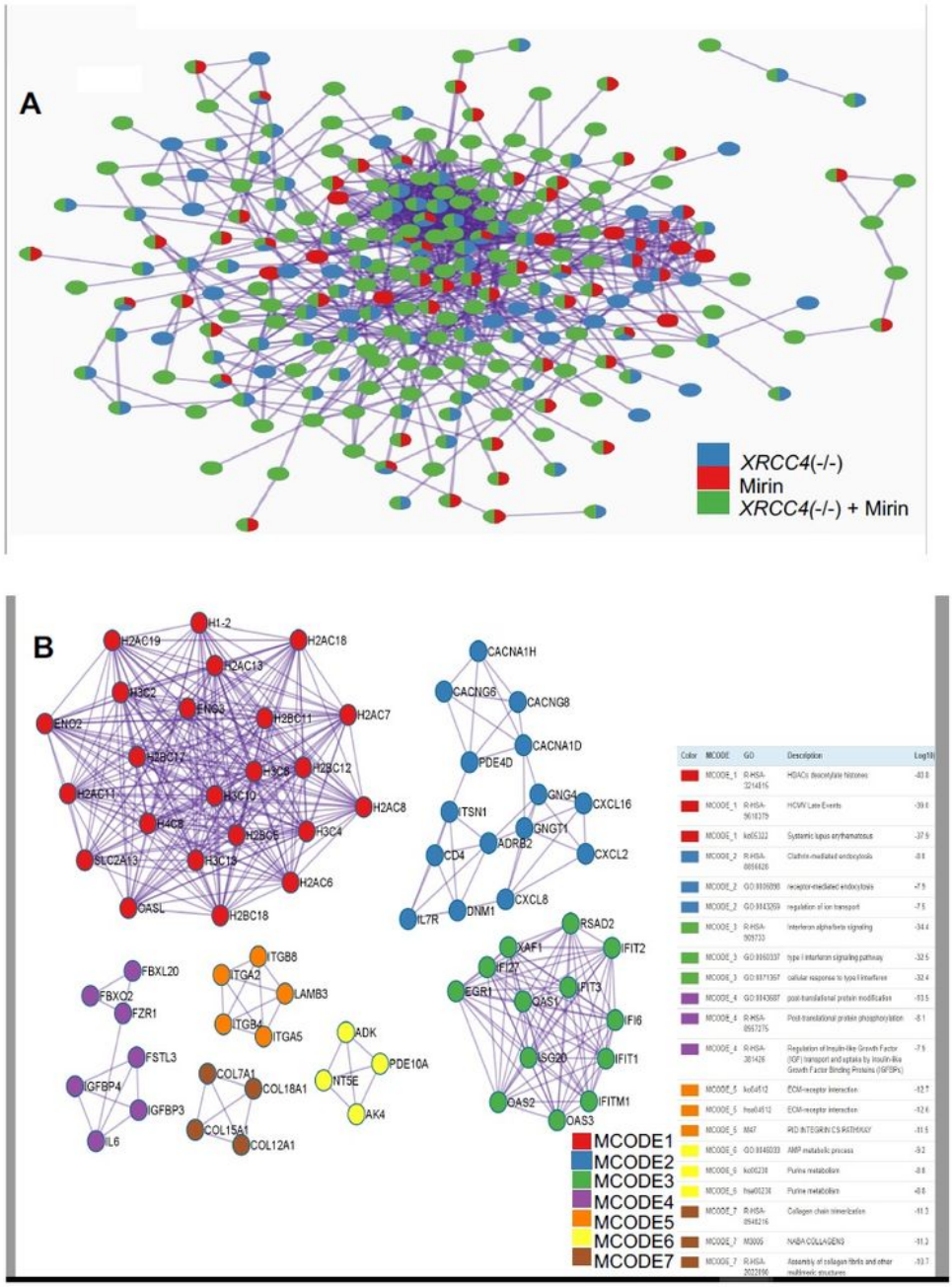

Figure 6

Protein-protein interaction network analysis. A) PPI network of DEGs across all three NHEJ categories. Nodes are displayed as pies to indicate NHEJ sample. B) MCODE components were identified from merged network for all samples. Each MCODE network is assigned a unique color and the network was generated with Cytoscape (v3.1.2). C) MCODE GO term, description and p values are shown.

Supplementary Files

This is a list of supplementary files associated with this preprint. Click to download.

- NHEJsuppfigures4.24.21.pdf
- SupplementaryTable1.xlsx
- SupplementaryTable2.xlsx